Feasibility of Noncontact Intracardiac Ultrasound Ablation and Imaging Catheter for Treatment of Atrial Fibrillation

Serena H. Wong, *Student Member, IEEE*, Greig C. Scott, *Member, IEEE*, Steven M. Conolly, Girish Narayan, and David H. Liang

***Abstract*—Atrial fibrillation (AF) affects 1% of the population and results in a cost of $2.8 billion from hospitalizations alone. Treatments that electrically isolate portions of the atria are clinically effective in curing AF. However, such minimally invasive catheter treatments face difficulties in mechanically positioning the catheter tip and visualizing the anatomy of the region. We propose a noncontact, intracardiac transducer that can ablate tissue and provide rudimentary imaging to guide therapy. Our design consists of a high-power, 20 mm by 2 mm, 128-element, transducer array placed on the side of 7-French catheter. The transducer will be used in imaging mode to locate the atrial wall; then, by focusing at that location, a lesion can be formed. Imaging of previously formed lesions could potentially guide placement of subsequent lesions. Successive rotations of the catheter will potentially enable a contiguous circular lesion to be created around the pulmonary vein. The challenge of intracardiac-sized transducers is achieving high intensities (300–5000 W/cm^2) needed to raise the temperature of the tissue above 43°C. In this paper, we demonstrate the feasibility of an intracardiac-sized transducer for treatment of atrial fibrillation. In simulations and proof-of-concept experiments, we show a 37°C temperature rise in the lesion location and demonstrate the possibility of lesion imaging.**

I. Introduction

Atrial fibrillation (AF) affects 1% of the U.S. population (320,000 new cases per year) and results in 465,000 hospitalizations per year [1]. AF increases the risk of stroke five-fold and is responsible for 15–20% of all strokes, reducing the quality of life[1].

AF is often treated with open-chest, surgical MAZE procedures, which control the propagation of electrical wavefronts in the atria using a series of patterned lesions. In most cases, these wavefronts originate from aberrant foci in the pulmonary veins [2]; isolating these electrical signals has been shown to prevent AF [3].

Recent trials suggest that minimally invasive circumferential pulmonary vein ablation (CPVA), in which contiguous lesions are placed around each pulmonary vein opening, isolates aberrant foci from the atria (Fig. 1) [4]. The success of CPVA depends on the completeness of isolation; when residual gaps in the lesions remain, the recurrence rate of AF increases [5], [6].

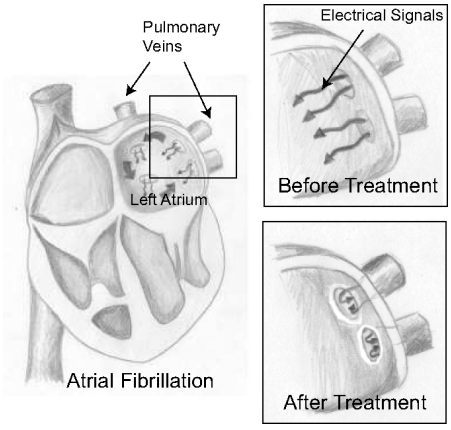

Fig. 1. In most cases, AF is caused by electrical signals entering the atria from the pulmonary veins (left)[1]. Before circumferential pulmonary vein ablation, these signals propagate from the pulmonary vein into the atria (top box). After treatment, these signals are isolated from the atria and cannot trigger AF (bottom box).

A. Challenges of Catheter Ablation

Widespread acceptance of ablative strategies for treating AF has been limited by the need for surgical intervention and the difficulty and limited success of minimally invasive catheter-based approaches [4]. Long-term success of catheter-based ablation is only 82%, despite the need for an average of 1.6 procedures per patient [7]. Catheter-based procedures are tedious, with procedure times longer than 4 hours, of which 1 hour is RF therapy application [8]. Also, because these procedures depend on fluoroscopy for visual guidance, they result in extensive radiation exposure. A recent study shows average fluoroscopy times of 68 minutes result in an effective organ dose of 27 mSv. This significant dose results in an estimated lifetime risk of one malignancy for every 500 procedures [9]. This motivates the development of a technique that relies on significantly reduced X-ray dose.

The two main challenges of catheter ablation are visualizing the desired location for lesion placement and positioning the therapy at the desired site.

1. Current Visualization Techniques: Current catheter procedures rely on two-dimensional (2-D) fluoroscopic pro-

Manuscript received August 5, 2005; accepted May 23, 2006.

The authors are with Stanford University, Department of Electrical Engineering, Stanford, CA (e-mail: shwong@stanford.edu).

Digital Object Identifier 10.1109/TUFFC.2006.188

[1]American Heart Association 2005 Update. http://www.americanheart.org/downloadable/heart/1105390918119HDSStats2005Update.pdf

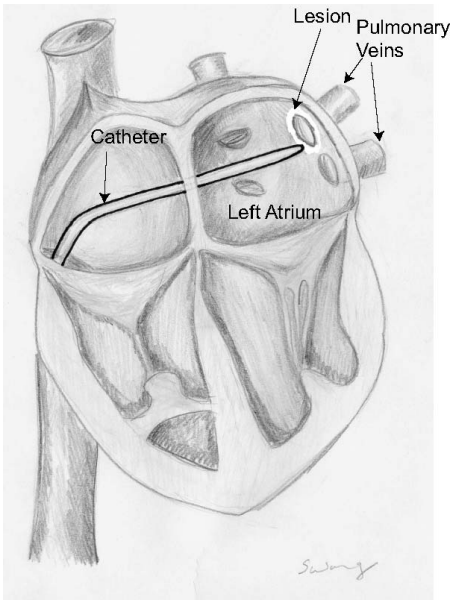

Fig. 2. Illustration of RF CPVA procedure. A catheter, inserted through the femoral vein, is passed through the inter-atrial septum into the left atria.

jection images with little soft tissue contrast. The anatomical structures relative to the catheter's position are hard to determine and contribute to the difficulty of directing the catheter to a specific site.

Groups have overlaid fluoroscopic images on preprocedural computerized tomography (CT)/magnetic resonance imaging (MRI) images to provide information on the catheter's position relative to atrial structures [10]–[12]. Electromagnetic sensing techniques have provided a 3-D coordinate system to identify prior catheter placement. However, the precision of these methods suffers from misregistration of the images due to cardiac and respiratory motion [13], [14].

Intracardiac ultrasound catheters, like AcuNav (Siemens Acuson, Malvern, PA) have been used to visualize anatomy. However, because the images are tomographic slices, identifying and guiding separate ablation catheters and imaging catheters requires coordinated motion and remains challenging [15].

A solution integrating an imaging system and ablation system onto the same catheter would potentially solve misregistration issues and eliminate the difficulty in guiding separate catheters.

2. Current Positioning Techniques: Lesions are typically made by direct contact of a catheter tip with the desired location for application of therapy. To reach the atrium, the catheter is passed from the femoral vein through the right atrium into the left atrium (Fig. 2). Motion to the catheter tip must be transmitted along a 110-cm flexible length. Motion control remains limited to rotating, advancing, and deflecting the catheter tip. With this crude control, it is difficult to revisit previous treatment locations or move to specific neighboring locations.

Attempts to address this issue have focused on developing fixed geometry devices to ablate rings around the pulmonary vein ostia [16]–[18]. These include balloon and lasso catheters that attempt to contact a circular ring of tissue at which therapy is applied. However, the highly variable geometry of the pulmonary veins (diameter 15 ± 10 mm, varied angulation, and shapes) limits the success of fixed geometry devices [19], [20]; often the entire device is not in continuous contact with the tissue.

A noncontact device that can dynamically steer therapy would aid positioning and compensate for motion and variable anatomy. If this device also could image anatomy and lesions without ionizing radiation, it would produce a more efficient procedure for treating AF.

B. Ultrasound Transducers for Ablation

The challenge of external ultrasonic ablation of cardiac tissue is the limited size of available acoustic windows. Subcutaneous fat and air in the lungs diminish the ultrasound energy that reaches cardiac tissues and impede noninvasive arrays [21]–[23]. Studies that use large spherical ablation transducers to deliver high-ablation intensities necessitate open-chest surgery [24]–[26].

Intracardiac placement of ablation transducers eliminates the difficulty of depositing power through layers of tissue and air. However, using peripheral vascular access limits the diameter of a device to 3–4 mm. This size limitation often constrains the configuration of catheter devices to rings and long rectangles and restricts the number and size of cables leading to the transducer. These wires limit the power safely deliverable to the transducer [27].

Contact intracardiac high intensity focused ultrasound (HIFU) transducers, such as small 2.3 by 5 mm transducers [28], [29] provide little benefit over RF electrodes as they require direct contact with the myocardium. Fixed geometry devices, such as balloon coupled transducers [17], [30],[2,3], suffer due to the highly variable geometry of the pulmonary vein ostia, which leads to inconsistent results.

Using a linear ultrasound array is advantageous because it can be focused and steered onto the region of interest, removing the need to create contact between the ablating device and tissue. Though the device diameter is limited to 3–4 mm, the length of the transducer can be as large as 20–30 mm; this larger length can potentially provide sufficient aperture and surface area needed to focus the beam tightly to ablate tissue. Though the use of larger arrays for HIFU has been proposed and demonstrated [31]–[34], a high aspect ratio, linear HIFU array for peripheral insertion has not been developed.

C. Ultrasound-Guided Ablation Devices

Ultrasound imaging arrays can provide real-time images of tissue to aid treatment of arrhythmias [35]–[37].

[2]Atrionix Company website. http://www.atrionix.com
[3]ProRhythm Company website. http://www.prorhythm.com/

Ultrasound imaging probes primarily have been used to guide HIFU transducers by displaying anatomy. Recent research also has demonstrated that ultrasound imaging can potentially detect past lesions as bright echogenic spots [24]; this brightness is proportional to HIFU intensity and fades within 1–2 minutes after HIFU application [38], [39]. Though lesion imaging is still under extensive research, it could potentially guide the placement of subsequent lesions. At the very minimum, an ultrasound device would be able to display the anatomy of the region, in particular the location of the atrial wall, to guide anatomical ablation (CPVA).

Several groups are developing intracardiac ultrasound catheters that combine ultrasonic imaging with a means for ablation. Sahn has developed a side-looking "hockey-stick" catheter with electrodes for monitoring intracardiac potentials [40], [41]. Although this device has shown high-quality images of cardiac structures, there are potential difficulties in localizing the treatment catheter and region of interest within the same imaging plane of the therapy catheter. Smith has designed an intracardiac ultrasound catheter that combines a 2-D imaging array with a fixed focus 4.5 mm diameter ablation ring [42]. Using 3-D ultrasound imaging to identify the region of interest, the catheter then is mechanically advanced to the desired ablation site. Although the image guidance improves the ability to perform precise ablations, achieving precise catheter motions to reach the desired ablation site remains challenging.

II. Proposed Device

Our proposed device is a dual-mode array, which will provide image guidance and electronically steerable therapy. The array is physically fixed and stabilized some distance from the heart wall using a balloon. Image feedback between applications of therapy could allow compensation for variable anatomy and motion during heart cycles (Fig. 3). An automated system with edge detection algorithms potentially could be used to automatically track the atrial wall to position the therapy. Because the blood-to-tissue contrast is great, typical postprocessing edge detection methods potentially could be used [43]. In addition, if a computer were tracking the edges and places of insonification, software could keep track of the treated regions of the heart.

The proposed design consists of a 20 mm by 2 mm, PZT 880 (APC International, Mackeyville, PA) on a 7 French catheter with a balloon stabilizing device. The 128 elements will be cut out of the 20-mm length with a diamond saw blade of 0.017 mm in thickness. A custom designed flex cable will connect each transducer to custom electronics. Direct digital synthesizers (DDS), AD9835 (Analog Devices, Sunnyvale, CA) with 12 bits of frequency resolution and 10 bits of phase resolution, will be used to alter the phase of each channel for focusing and steering. The DDS signal then is amplified and delivered to the transducer.

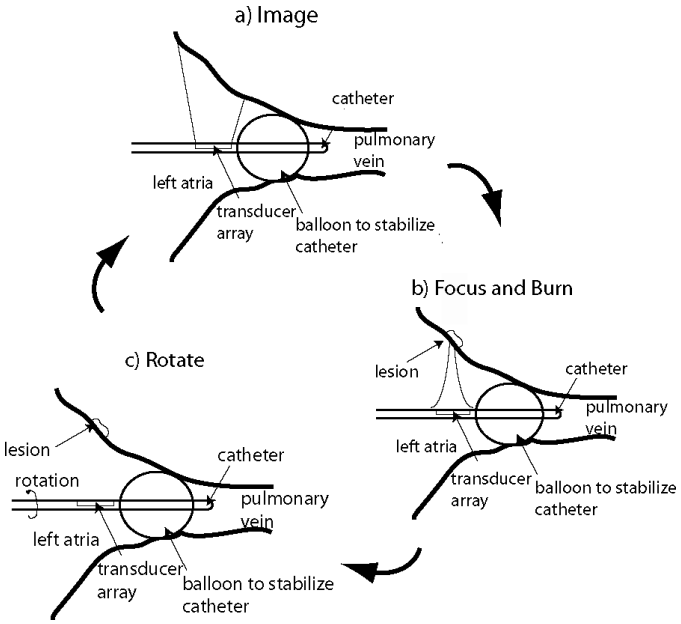

Fig. 3. An illustration of the catheter in action. (a) The array will image the region of interest. (b) The anatomy and location of previously formed lesions will be identified and used to dynamically focus the therapy. (c) The catheter will be rotated, and the process will repeat until a contiguous, circumferential lesion is formed around the pulmonary vein.

A two-channel prototype system controlled by a computer running LabView (National Instruments, Austin, TX) has been built (Fig. 4). Each channel outputs a maximum of 1 W into 50 Ω, with 30 dB harmonic suppression.

This system and device will provide a new approach to the anatomical treatment of atrial fibrillation. To show the feasibility of using such a small transducer for ablation, we demonstrate that focal intensities of 300–5000 W/cm^2 needed for ablation can be achieved [28], [44]–[46]. We calculated the beam profiles and resulting temperature rise from our transducer given that our transducers were specified to be able to output in excess of 30 W/cm^2 (information given by APC International, Mackeyville, PA). We found our transducer to have a focal intensity greater than 450 W/cm^2.

We then used a proof-of-concept, fixed-focus system to create these focal intensities and ablate tissue. To demonstrate potential for ultrasonic lesion monitoring, these fixed focus lesions also were imaged using conventional ultrasound to show that the HIFU lesion could potentially be visualized as a highly echogenic region.

III. Simulation

We simulated our array design to determine the beam profile and focal intensity of a small, intracardiac transducer. Then, using thermal models, we calculated the time required for necrosis for various focal intensities.

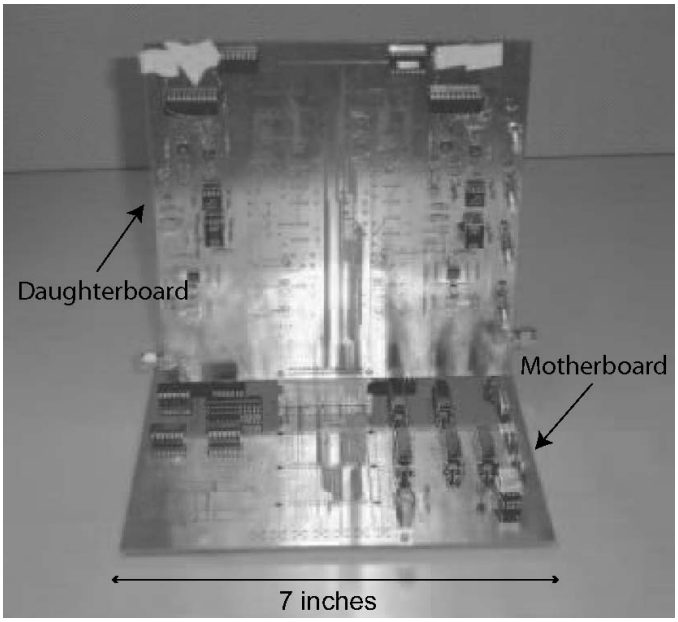

Fig. 4. Our prototype HIFU electronics system.

A. Materials and Methods

To determine the focal intensities of the array, we used Matlab (Mathworks, Matick, MA) to simulate the beam profile using Huygen's principle, which estimates each array element as a collection of point sources [47], [48]. The pressure due to each point source is given by:

$$p_i(x,y,z) = \sqrt{\frac{2W\rho}{cA}}\frac{fS}{d}e^{((\phi-2\pi d/\lambda)i-d\alpha)}, \tag{1}$$

where W is the total acoustic power from the array, A is the area of the array, S is the area of each source, ρ is the density (998 kg/m^3), c is the speed of sound (1500 m/s), f is the frequency, λ is the wavelength, and d is the distance from the simple source to the point of interest [48]. Ultrasound will be attenuated by intervening blood with an attenuation constant of 0.14 dB/cm/MHz [49]. The phase of each element was calculated using the expression given by Macovski [50]:

$$\tau_n = \frac{\beta n d}{c} - \frac{(nd)^2}{2zc}, \tag{2}$$

where β is the deflection angle, z is the focal length, n is the transducer element, and d is the transducer element spacing (Fig. 5). The total pressure at each point from all these simple sources was calculated by summing all the simple sources:

$$P(x,y,x) = \Sigma p_i(x,y,z). \tag{3}$$

The Ultrasim package (University of Oslo) for Matlab also was used to construct beam profiles and contour plots. We assumed the transducer was able to output in excess of 30 W/cm^2 (PZT 880 specification by APC International). The average intensity, I, was calculated by spatially averaging the intensity over the area enclosed by the half-pressure contour in the focal plane [46].

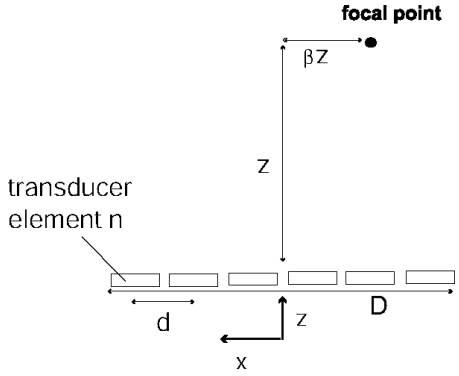

Fig. 5. An illustration depicting the coordinate system for calculating the transducer delays needed to focus at a particular point.

Temperature rises were calculated using COSMOSWorks (SolidWorks, Concord, MA). The region in which ablative power was deposited was simulated as a half ellipsoid in a piece of tissue with dimensions determined by the half pressure contours in the beam profile simulations. This lesion was placed at the surface of a larger 2-cm cubed tissue sample. The size of this larger cube was determined as adequate by decreasing and increasing the cube size incrementally and seeing that the temperature distribution remained similar. The intensities were converted to power per unit volume using the following equation, where α is the absorption of tissue, 0.5 dB/cm [42], [51], and I is the average intensity in the focal region determined by the half pressure contour in the focal plane:

$$\langle q \rangle = 2\alpha I. \tag{4}$$

The effects of perfusion were neglected since Billard *et al.* [52] showed that lesions under 3 mm in size formed in about 2 seconds have temperature rises that are not greatly affected by perfusion. Convection will be the dominant cooling force. Average convection coefficients in the left atrium range from 500–5350 W/m^2 K [53], [54]. Tangwongsan *et al.* [53] calculated a medium convection coefficient of 5350 W/m^2 K by averaging the convection coefficient over 30 seconds in the heart cycle and carefully positioning the sensor to face the blood flow; though this value is much higher (by 5–10 times) than previously measured convection coefficients, we will use it because it was the most carefully measured and gives the "worst-case" scenario. This convective surface was used as one boundary condition. Because we assume that most of the heating is occurring in the lesion area, the other boundaries were held at 37°C. An initial temperature of 37°C was used and step size of 1 ms.

After calculating the temperature, we determined tissue necrosis by using the cumulative equivalent minutes at 43°C (CEM$_{43}$) [55]. This metric determines tissue death by estimating total temperature dose over time and is expressed as the following, where $T(t)$ is temperature over time:

$$\mathrm{CEM}_{43} = \sum_{t=0}^{t=\mathrm{final}} R^{(43-T(t))} \triangle t, \tag{5}$$

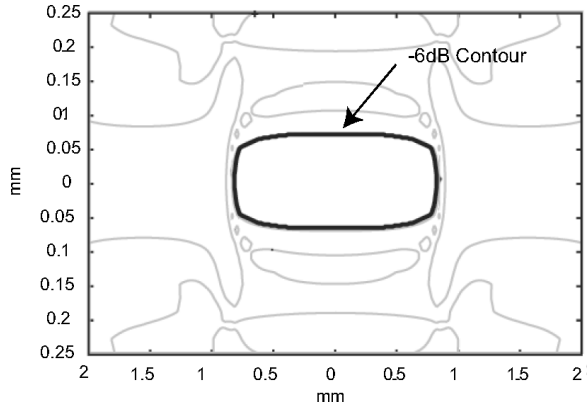

Fig. 6. Our simulated contour plot of normalized power (dB) in the focal plane. The −6 dB contour shows the area that receives a power gain of 32.

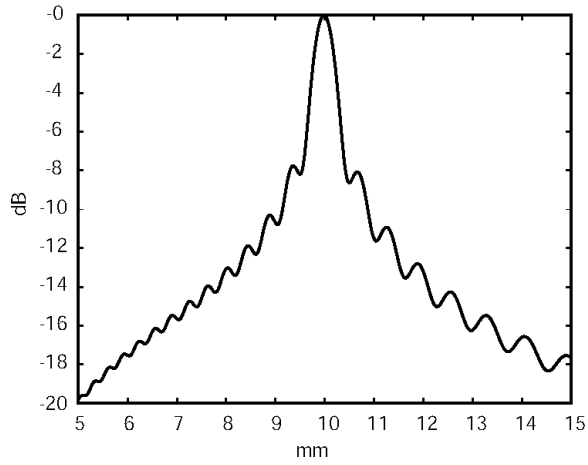

Fig. 7. Our simulated axial beam profile of normalized power (dB) when focusing to 10 mm.

where $R = 0.25$ if $T(t) < 43$ and $R = 0.5$ if $T(t) > 43$. Using the CEM_{43} threshold for myocardial necrosis of 128 minutes [56], we found the time at which necrosis occurs for a given focal intensity.

B. Beam Profile

Given that typical hard piezoceramics can output in excess of 30 W/cm^2, we simulated our transducer to show it can deliver greater than 300 W/cm^2 to the focal spot. We chose a 10 MHz operating frequency as it allowed tight focusing, but it was not limited by the absorption of blood between the transducer and tissue [57]. Focusing to 10 mm on-axis, the power gain was 65 and a spatial time average of 900 W/cm^2 was deposited within the −6 dB contour (Fig. 6); secondary maxima were suppressed by 12 dB. Fig. 7 shows the −6 dB axial beamwidth to be 1 mm, which is slightly smaller than the thickness of the atrial wall (1.5–3 mm) [58].

Lateral steering of 5 mm and adjustable focal depths of 5–15 mm allows compensation for cardiac motion near the pulmonary vein and variable pulmonary vein diameter

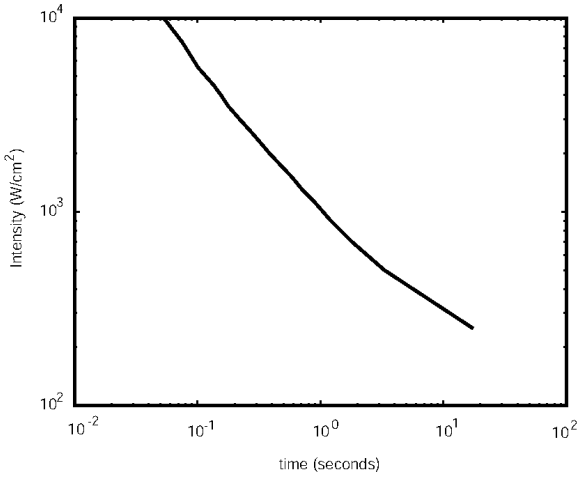

Fig. 8. Our calculated threshold intensities for ablation of tissue within a given time. Perfusion was neglected, but convection was assumed to be 5350 W/m^2 K.

$(15 \pm 10$ mm). Focusing to depths between 5 and 17.5 mm with high gain and 6 dB suppression of secondary maxima was achievable. Grating lobes, which result from aliasing when transducer elements are more than $\lambda/2$ spacing apart, became a challenge when steering more than several millimeters off-axis. The contribution to these lobes was mostly from elements at the edge of the array.

C. Heating Threshold and Tissue Necrosis

RF ablation has long heating times (>30 seconds), which is disadvantageous in the constantly moving environment of the heart. RF ablation times are long to prevent the charring, coagulation, and shallow lesions characteristic of high power/fast RF application. Ultrasound lesions can be produced much more quickly than RF lesions without the threat of coagulation.

In lesion formation, the limiting factor is the tissue at the very surface of the myocardium because it is subjected to the greatest cooling from flowing blood. With this in mind, we determined the threshold times for necrosis based on the temperature rise at the very surface of the lesion for intensities between 250–10,000 W/cm^2 (Fig. 8). For tissue at the surface of the myocardium, necrosis occurs anywhere from 65 milliseconds at 10,000 W/cm^2 to 17 seconds at 250 W/cm^2.

Motion within the heart presents a challenge to the application of therapy. Even the motion of about 1 mm near the pulmonary veins will disturb the heating process. Because the heart may be in fibrillation, the position of the myocardium may not have a regular cycle; thus, we will use a motion-tracking scheme to dynamically adjust focus of therapy.

The distance to myocardial structures or locations of lesions will be observed by m-mode every 60–65 ms (15 Hz refresh rates are typical for echocardiograms), and the focus of the therapy will be dynamically adjusted to compensate (Fig. 9). Ablation will be fairly continuous and

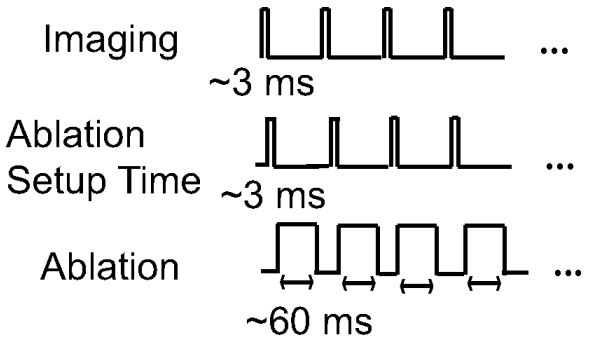

Fig. 9. Anatomical tracking and gating scheme. The location of the heart wall is assessed every 60 ms and adjusted.

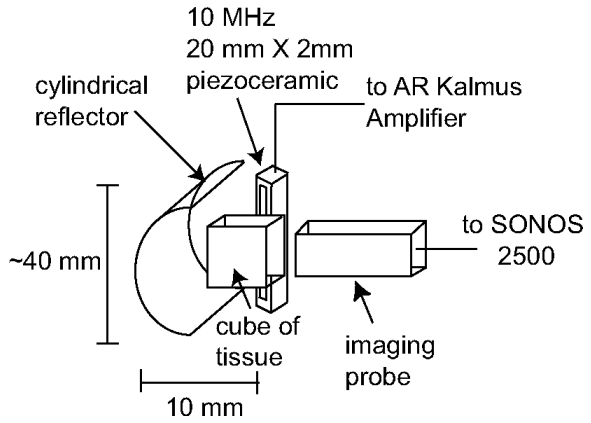

Fig. 10. A 10 MHz, 20 mm by 2 mm transducer was used for fixed focus ablation, using a cylindrical mirror (focal length of 10 mm). The transducer was angled to produce an off-axis lesion in a piece of tissue. Running water was pumped over the tissue to simulate convection from blood. A 0.25 mm diameter microthermocouple was placed inside the tissue to measure the temperature rise at the focal point. The lesion was imaged using a 5 MHz SONOS 2500 ultrasound probe.

interlaced with 6 ms periods for imaging and refocusing. The first 3 ms of this period comes from the image acquisition. Assuming the speed of sound to be 1580 m/s and a total travel distance of 20 mm to the myocardium wall, the time required is roughly 12 μs. If all the elements transmit, then each element receives individually, this will be 128 two-way distances, which equals roughly 3 ms. Our electronic focusing system, described above, requires about 2 ms to calculate and reprogram the delays, leaving 1 ms for computer calculation. Tissue cooling is negligible because, during the 6 ms when the therapy is off, the tissue will retain about 98–99% of its heat. Assuming ablation pulses have a high-duty cycle, the time to necrosis will approximate the curve shown in Fig. 8. From this curve, we can predict that our array, which produces focal intensities of at least 450 W/cm^2, will cause tissue necrosis in less than 5 seconds. These conclusions seem consistent with ultrasound thresholds found by other researchers [44], [45].

IV. Proof-of-Concept In Vitro Experiments

To reduce the complexity of developing a full array system, in our preliminary experiments we used a fixed focus setup to show that an intracardiac-sized transducer could create temperature rises to induce tissue necrosis in several seconds. We also showed that the HIFU lesions could be visualized under ultrasound imaging.

A. Methods and Experimental Setup

A fixed-focus system could be constructed either using a lens or a fixed-focus reflector. Although a lens would allow us to perform on-axis simulations, a large radius of curvature was needed because we were focusing so close to the transducer. With silicone or plastic to make such a lens, the attenuation through a large thickness at 10 MHz would greatly attenuate the acoustic wave. Hence, we decided to use a reflector design, although we would have to place the tissue very slightly off axis.

The fixed-focus system consisted of a (20 mm by 2 mm) single element transducer (APC 880, APC International, Ltd.) and a focusing cylindrical reflector (10 mm focal length). We positioned the tissue at the reflector's focal point and angled the transducer to produce an off-axis lesion (Fig. 10). We submerged the setup in running 21°C water and applied a 10 MHz, 10 W CW signal to the transducer.

We measured temperatures at the focal point with a Type E, 0.25 mm diameter micro-thermocouple (Omega, Stamford, CT). Because the duty cycle of the ablation pulses should be close to 100%, we decided to study the effects of continuous therapy application. We also characterized the lesion shape using a HIFU gel [59]. This gel changes from clear to opaque at 55°C. An HP SONOS 2500, 5 MHz imaging probe (Hewlett-Packard, Sunnyvale, CA) was placed along the direction of propagation to image the lesion in real-time.

B. Fixed Focus In Vitro Ablation Results

We measured a 37°C temperature rise in a piece of tissue (Fig. 11). This corresponds to a focal intensity of 250 W/cm^2 and off-axis gain of 20. The calculated CEM_{43} (Fig. 12), after the base temperature is scaled to 37°C, shows tissue necrosis occurs between 3 and 4 seconds, in contrast with the 30 or more seconds required in RF ablation.

The times for necrosis are less than those calculated above; this is because the threshold determined above was based on the tissue at the surface of the lesion, which experiences more convective cooling. In our fixed focus experiments, we measured temperatures at the center of lesion (about 1 mm from the surface of the tissue).

Though these intensities could ablate tissue, ideally lesions will be produced in under a second to coincide with diastole, when there is minimal motion and convective flow.

We characterized the lesion shape and size in a piece of tissue and also using a HIFU gel [59], which allowed us

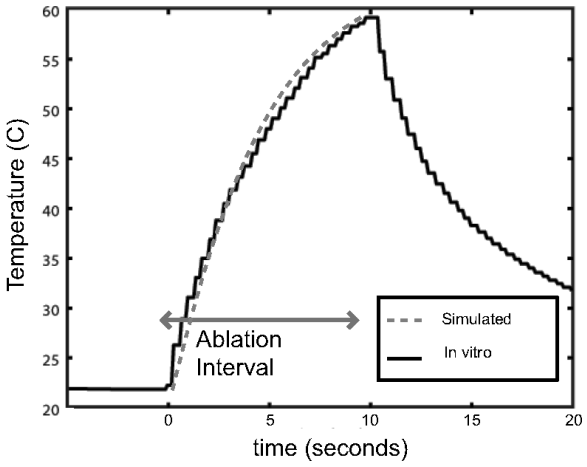

Fig. 11. Temperature rise in a piece of tissue measured by a type E microthermocouple. A 10 W, 10 MHz CW, 10 second signal was applied to the transducer in our fixed-focus setup (Fig. 10). A temperature rise of 37°C was observed.

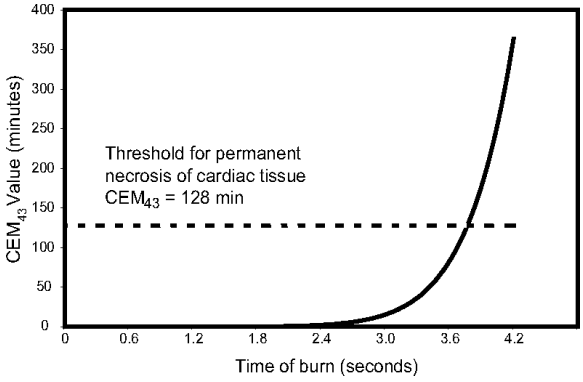

Fig. 12. Calculated CEM_{43} for the temperature profile measured in our HIFU setup (Fig. 11). Tissue necrosis occurs at 3.8 seconds at a CEM_{43} of 128.

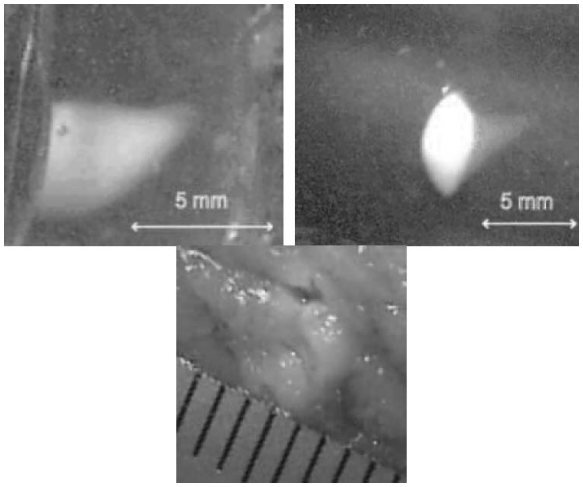

Fig. 13. (Top) Pictures of a HIFU lesion formed by our fixed-focus system (Fig. 10) in the focal plane (right) and along the direction of propagation (left) formed in a HIFU gel that changes from clear to opaque at 55°C. (Bottom) Cross-sectional view lesion in actual beef tissue is shown to be approximately the same size as in the gel.

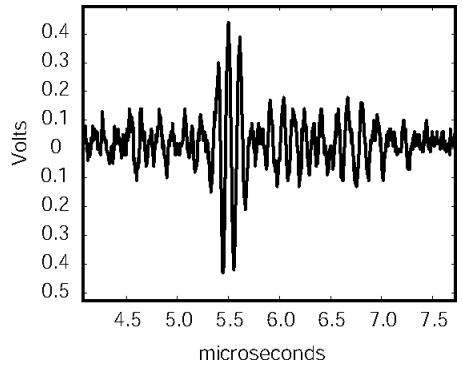

Fig. 14. Pulse-echo response from a wire phantom placed 1 cm from the surface of 2 mm by 0.3 mm PZT 880 transducer. As seen, the ring-down is significant (about 20 cycles), but the front surface of the wire is clearly visible from the first echo.

to see the full lesion without the difficulty of sectioning tissues. The 55°C contour of the lesion is 1 mm by 3 mm in the focal plane, and the lesion depth is 4 mm (Fig. 13). The lesion dimensions of 3 mm indicates that about 50 lesions will be needed for a continuous ring encircling the pulmonary veins, for a total treatment time of 3–4 minutes.

C. Imaging for Guidance of Ablation

As indicated in the introduction, ultrasound imaging can be used to identify the region of interest anatomically and potentially identify past lesion locations. Though a high Q transducer will provide good power transfer to ablate tissue, it will exhibit a long ring-down when used for imaging. For anatomical imaging, however, the primary goal is to identify the atrial wall, which is located at the first echo in an image. The consequential ringing will not affect this parameter.

Using a 2 mm by 0.3 mm slice of PZT 880, we performed a 10 MHz, pulse-echo A-scan of a 1 mm diameter wire phantom placed 1 cm from the surface of the transducer (Fig. 14). As seen, there is a long ring-down, which limits axial resolution; however, the front surface of the wire is clearly visible from the first large echo. With regards to anatomical imaging, limited axial resolution is acceptable because we are interested only in the distance to the atrial wall, which is measured by the first echo in an A-scan. This first echo will be large from the impedance change between tissue and blood.

A second use of ultrasound imaging, which is the subject of current research, is the visualization of lesions, which potentially can be used to guide subsequent lesion placement. Because we have not yet developed a HIFU array and imaging system, we explored whether lesions produced by our fixed focus system could be visualized under ultrasound imaging using a SONOS probe.

Using the setup of Fig. 10, we imaged a HIFU lesion in real-time for 2 minutes and observed a 33% increase in brightness at the lesion location after the HIFU application. This brightness faded 30–45 seconds after HIFU

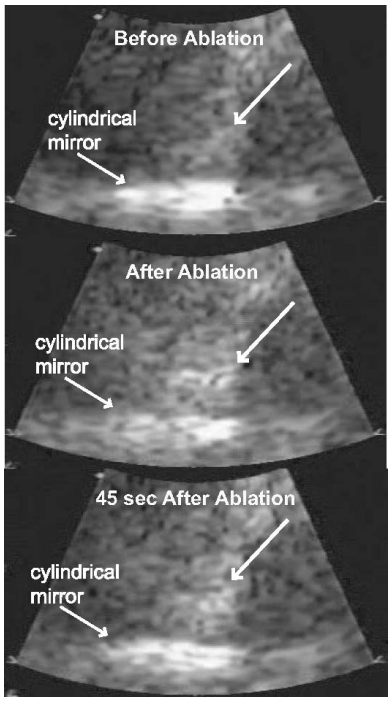

Fig. 15. Series of real-time images taken by a SONOS 2500, 5 MHz probe of a fixed-focus HIFU lesion. The brightness of the lesion increases 33% from before (top) to after (middle) HIFU application. The brightness then decays over a 45 second interval (bottom).

application (Fig. 15). This echogenicity is attributed to nonlinear heating and outgassing and is correlated with HIFU intensity [38], [60].

Although the imaged lesions fade quickly, they potentially provide real-time feedback for placement of successive lesions, essential for constructing contiguous patterns. Although a typical imaging transducer could image the lesions effectively, the ring-down of the high Q, therapeutic transducer will reduce imaging resolution. With regard to imaging lesions, the ring-down can be potentially treated using methods by other groups working in dual-mode ultrasound and is addressed in the discussion section.

V. Discussion

According to our simulations, our ultrasound transducer can produce intensities of 450–900 W/cm^2 at the focal point in cardiac tissues. Using these intensities, we calculated that tissue necrosis would occur in less than 10 seconds, taking into account convection from the blood. We have neglected perfusion, which may cause additional tissue cooling and lengthen the needed duration for necrosis.

Although the curved or irregular surface of the atrial wall will affect our beam profile because it is a phase aberrator, we did not include this in our calculations. Because the face of the atrial wall is variable from person to person, it was difficult to include a typical curvature for our calculations. In general, the effect of the curved interface is to distort the beam profile by refraction. Consequently, this could reduce the power density in the focal point. Reduction of the power density potentially could lengthen the duration of therapy needed for necrosis.

Out of plane motions also will affect the heating and formation of a particular lesion. If the patient has normal cardiac sinus when applying therapy, the easiest way to address motion is to apply therapy during diastole, when the heart remains relatively still. Ideally, if a lesion were formed within this time frame of about 100 ms, which would require intensities of greater than 1000 W/cm^2, the out-of-plane motions would be less of a concern. If lesions were formed at the same time within every heart cycle and we assumed the heart returned to roughly the same shape every heart cycle, we also would have reasonable certainty of where the ablated regions are located. Additionally, imaging will provide some crude anatomical locators to help detect these out of plane rotations. With such indicators, these rotations could be detected and potentially accounted for.

However, if the patient's heart is fibrillating, motion will be more unpredictable, which will make compensation and tracking more difficult. Previously, we described an automated system that tracks the heart wall and alternately images after applying therapy for several seconds. If the heart motion is faster than the application time, the lesion will be placed in the wrong location. A safety limit for therapy duration and maximal allowable position miscalibration should be determined. We will need to develop more complex finite-difference time domain heating models that allow time-dependent and location-dependent application of therapy in the tissue. Additionally, we will need to do more detailed clinical observation to analyze atrial wall movement during fibrillation in order to fine tune a tracking and therapy system that will be reasonably accurate. Using this information, we also can establish a therapy miscalibration and duration safety limit.

We also have neglected the nonlinear response of tissue to heating. When tissue is heated, there is a nonlinear increase in tissue absorption. This will cause most of the energy to be deposited at the front of the lesion (axially), forming shallow, "tadpole"-shaped lesions. We also have neglected the effects of outgassing and cavitation, which are not significant for 10 MHz until over 1000–3000 W/cm^2 is applied. The increase in absorption and cavitation effects actually will increase the energy deposited in the tissue and increase the ability to necrose tissue. However, the lesion shape and lesion depth will be different than expected. This may be accounted for by adjusting the focal depth within the myocardium wall at various portions of the treatment.

Additionally, we have not explored the effects of lesion-to-lesion interaction and spacing or accounted for these effects in simulations. The residual heat and bubbles formed by previous lesions could affect the shape and size of successive lesions, preventing the formation of successive lesions or causing damaging cavitational effects. However, given sufficient cooling time, a contiguous lesion pattern can be formed [61]. Luckily, blood flow within the heart

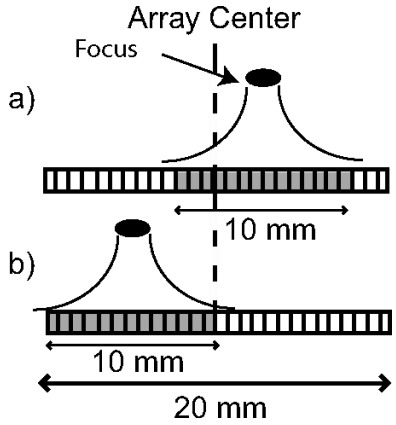

Fig. 16. Illustration of choosing different subarrays for treating regions at large lateral distances from the center of the array. Because the subarray is chosen so the focus is on axis, problems with grating lobes approaching the intensity of the main lobe when steering off-axis will be overcome. The system still retains a focal gain of 30 or more.

serves to effectively cool the area. Further in vivo experiments will need to be conducted to optimize the lesion-to-lesion spacing and cooling period needed between lesions to produce contiguous patterns of lesions. If long cooling times are needed, the lesion location may no longer be visible under ultrasound imaging. In this case, an automated system could be used to remember and track the location of past lesions.

We also have not addressed ultrasound safety in our simulations. Perforation of the atrial wall is a concern. However, because the axial beamwidth is about one-third to three times smaller than the atrial wall width [8], perforation should not be a large problem. Unwanted thermal damage from the side lobes in the beam pattern also may be a concern. The side lobes are suppressed by 12 dB; and given the duration of the insonification, the damage should be limited. However, these concerns of the threshold safety dose in the heart and the safety of our devices will be evaluated in further experiments.

Increasing the array's lateral steering will allow greater compensation for motion, and thus more effective therapy. In our current array, the side lobe levels became greater when steering more than several millimeters off axis. Most of the contribution to these side lobes is from the side elements. By switching those elements off and using a subarray approach, we could reduce the grating lobes under −10 dB, though reducing gain to 30. These subarrays can be chosen such that the point of interest is on-axis (Fig. 16). Because the subarray does not have to be steered off-axis, the grating lobe levels will remain low compared to the main lobe. The decreased aperture will decrease the maximum gain at most by a factor of 2. With the same input power to the elements, this means the focal intensity will be reduced to 450 W/cm^2, which still could be used for ablation. Further simulations and experiments have to be performed to determine the effectiveness and safety of this method.

In our in vitro experiments, we also have demonstrated the formation of lesions from these intensities. Though the intensities formed by our transducer are rather low, ablation is still possible.

The output power of the transducer could be greatly improved to increase the focal intensity. Our current transducer is very inefficient. At 10 MHz, we measured a peak output pressure of 0.8 MPa (20 W/cm^2) at the transducer's surface; we did this by measuring the pressure a certain distance from the transducer surface, then correcting for attenuation of water and diffraction [62]. The efficiency (20%) was lower than desired because of the high impedance of the backing layers. If we change our impedance backing from nickel to air, the change in impedance alone should allow an increase in reflection coefficient from 30% to nearly 100%, which could increase our efficiency to about 60%. This could greatly increase the focal power and rate of tissue necrosis.

Additionally, the lesions we formed were off-axis because of the physical arrangement of the components in the setup. On-axis lesions should have higher gains and thus higher intensities at the focal point. Also, convection occurred from all sides of the tissue instead of at the very surface of the tissue as is the case in the heart, which may have caused increased cooling.

With the increase in focal intensity, lesions can be created faster and can be imaged better because the brightness and persistence of the lesion are highly dependent on focal intensity.

Although imaging using a high-Q transducer is difficult because the ring-down of the transducer will reduce resolution, anatomical imaging guidance should be possible as we are mostly interested in locating the surface of the atrial wall. Although the transducer will have long axial ring down, the atrial wall should be visible as the first bright echo. With regard to lesion imaging, reduction of ring-down will definitely benefit the image quality. Simon *et al.* [63], have shown that a therapeutic piezocomposite array could be used for imaging. They used a low Q series inductor to reduce the ring-down and improve the frequency response. Using an approach similar to this, we potentially can reduce ring-down to produce lesion images capable of guiding therapeutic applications. Additionally, in the design of the PZT materials, tradeoffs can be made between power transmission (high mechanical Q) and image quality/resolution. These issues are currently a subject of on-going research.

With the goals to improve therapeutic output and imaging capabilities of our array, we will continue to develop a device that can be inserted on a catheter for in vivo testing. With the development of this device, we can test lesion-to-lesion interaction, pulsing effects, and other nonlinear heating and mechanical effects.

VI. Conclusions

We have simulated and designed a transducer array to produce focal intensities that can potentially cause tis-

sue necrosis. In in vitro fixed-focus experiments, we have demonstrated that an intracardiac-sized transducer can achieve the temperatures needed to reach the necrosis threshold of CEM_{43} equal to 128 minutes in less than 4 seconds. These lesions also were shown to be visible under conventional ultrasound; with the development of a tracking and automated system, these images could not only provide anatomical feedback, but also potentially could provide feedback on locations of therapeutic application. We are currently developing the full-fledged array systems and have prototyped much of the electronics, software, and transducer design. With this system, we can proceed with in vitro and in vivo testing and exploration of the effects of HIFU on tissue.

Acknowledgments

The authors would like to thank Professors John Pauly and Albert Macovski for their helpful advice and support.

References

[1] A. S. Go, E. M. Hylek, K. A. Phillips, Y. Chang, L. E. Henault, J. V. Selby, and D. E. Singer, "Prevalence of diagnosed atrial fibrillation in adults: National implications for rhythm management and stroke prevention: The anticoagulation and risk factors in atrial fibrillation (ATRIA) study," *JAMA*, vol. 285, pp. 2370–2375, 2001.

[2] M. Haïssaguerre, P. Jaïs, D. C. Shah, A. Takahashi, M. Hocini, G. Quiniou, S. Garrigue, A. Le Mouroux, P. Le Métayer, and J. Clémenty, "Spontaneous initiation of atrial fibrillation by ectopic beats originating in the pulmonary veins," *N. Engl. J. Med.*, vol. 339, pp. 659–666, 1998.

[3] M. Haissaguerre, D. C. Shah, P. Jais, M. Hocini, T. Yamane, I. Deisenhofer, S. Garrigue, and J. Clementy, "Mapping-guided ablation of pulmonary veins to cure atrial fibrillation," *Amer. J. Cardiol.*, vol. 86, Suppl 1, pp. K9–K19, 2000.

[4] A. M. Gillinov, P. M. McCarthy, N. Marrouche, and A. Natale, "Contemporary surgical treatment for atrial fibrillation," *Pacing Clin. Electrophysiol.*, vol. 26, pt. 2, pp. 1641–1644, 2003.

[5] K. Seidl, H. Schwacke, R. Zahn, M. Rameken, A. Drogemuller, and J. Senges, "Catheter ablation of chronic atrial fibrillation with noncontact mapping: Are continuous linear lesions associated with ablation success?," *Pacing Clin. Electrophysiol.*, vol. 26, pt. 1, pp. 534–543, 2003.

[6] S. Ernst, F. Ouyang, F. Löber, M. Antz, and K. Kuck, "Catheter-induced linear lesions in the left atrium in patients with atrial fibrillation: an electroanatomic study," *J. Amer. Coll. Cardiol.*, vol. 42, pp. 1271–1282, 2003.

[7] A. Goldberg, M. Menen, S. Mickelsen, C. MacIndoe, M. Binder, R. Nawman, G. West, and F. M. Kusumoto, "Atrial fibrillation ablation leads to long-term improvement of quality of life and reduced utilization of healthcare resources," *J. Interv. Cardiol. Electrophysiol.*, vol. 8, pp. 59–64, 2003.

[8] R. Mantovan, R. Verlato, V. Calzolari, S. Baccillieri, A. De Leo, P. Turrini, G. Pastore, M. Crosato, A. Ramondo, and P. Stritoni, "Comparison between anatomical and integrated approaches to atrial fibrillation: Adjunctive role of electrical pulmonary vein disconnection," *J. Cardiovasc. Electrophys.*, vol. 16, pp. 1293–1297, Dec. 2005.

[9] L. Lickfett, M. Mahesh, C. Vasamreddy, D. Bradley, V. Jayram, Z. Eldadah, T. Dickfelf, D. Kearney, D. Dalal, B. Luderitz, R. Berger, and H. Calkins, "Radiation skin exposure, effective organ doses, and estimated cancer risk for pulmonary vein and cavotricuspid isthmus ablation using a low frame pulsed fluoroscopy system," *J. Amer. Coll. Cardiol.*, vol. 43, Suppl. A, pp. 1009–1221, 2004.

[10] V. Reddy, Z. Malchano, G. Holmvang, E. J. Schmidt, A. D'Avila, C. Houghtaling, R. C. Chan, and J. N. Ruskin, "Integration of cardiac magnetic resonance imaging with three-dimensional electroanatomic mapping to guide left ventricular catheter manipulation: Feasibility in a porcine model of healed myocardial infarction," *J. Amer. Coll. Cardiol.*, vol. 44, pp. 2202–2213, 2004.

[11] T. Dickfeld, S. B. Solomon, H. Calkin, M. Issa, and K. Lemola, "Anatomic stereotactic catheter ablation on three-dimensional magnetic resonance images in real time," *Circulation*, vol. 108, pp. 2407–2413, 2003.

[12] S. B. Solomon, R. Lederman, M. Guttman, T. Dickfeld, and S. Han-Haim, "Real-time cardiac catheter navigation on three-dimensional CT images," *J. Interv. Cardiol. Electrophysiol.*, vol. 8, pp. 27–36, 2003.

[13] S. Shpun, L. Gepstein, G. Hayam, and S. A. Ben-Him, "Guidance of radiofrequency endocardial ablation with real-time three-dimensional magnetic navigation system," *Circulation*, vol. 96, pp. 2010–2016, 1997.

[14] G. Hayam, L. Gepstein, and S. A. Ben-Haim, "Accuracy of the in vivo determination of location using a new nonfluoroscopic electroanatomical mapping system," *Pacing Clin. Electrophysiol.*, vol. 19, pt. 2, pp. 712–718, 1996.

[15] L. Zheng, D. McCormick, I. Dairywala, S. Surabhi, and S. Goldberg, "Catheter-based intracardiac echocardiography in the interventional cardiac laboratory," *Catheter. Cardiovasc. Interven.*, vol. 63, pp. 63–71, 2004.

[16] M. D. Lesh, P. Guerra, F. X. Roithinger, Y. Goseki, C. Diedrich, W. H. Nau, M. Maguire, and K. Taylor, "Novel catheter technology for ablative cure of atrial fibrillation," *J. Interv. Cardiol. Electrophysiol.*, vol. 4, Suppl 1, pp. 127–139, 2000.

[17] M. D. Lesh, C. Diederich, P. G. Guerra, Y. Goseki, and P. B. Sparks, "An anatomic approach to prevention of atrial fibrillation: Pulmonary vein isolation with through-the-balloon ultrasound ablation," *Thorac. Cardiovasc. Surg.*, vol. 47, pp. 346–351, 1999.

[18] B. Avitall, R. W. Helms, J. B. Koblish, W. Sieben, V. Kotova, and G. N. Gupta, "The creation of linear contiguous lesions in the atria with an expandable loop catheter," *J. Amer. Coll. Cardiol.*, vol. 33, pp. 972–984, 1999.

[19] M. Mansour, G. Holmvang, D. Sosnovik, R. Migrino, S. Abbara, J. Ruskn, and D. Keane, "Assessment of pulmonary vein anatomic variability by magnetic resonance imaging: Implication for catheter ablation techniques for atrial fibrillation," *J. Cardiovasc. Electrophysiol.*, vol. 15, pp. 387–393, 2004.

[20] E. M. Marom, J. E. Herndon, Y. H. Kim, and H. P. McAdams, "Variations in pulmonary venous drainage to the left atrium: Implications for radiofrequency ablation," *Radiology*, vol. 230, pp. 824–849, 2004.

[21] E. S. Ebbini, J. C. Bischof, and J. E. Coad, "Lesion formation and visualization using dual-mode ultrasound phased arrays," in *Proc. IEEE Ultrason. Symp.*, 2001, pp. 1351–1354.

[22] E. S. Ebbini, C. Simon, H. Lee, and W. Choi, "Self-guided ultrasound phased arrays for noninvasive surgery," in *Proc. SPIE*, 2001, pp. 30–40.

[23] H. Yao, P. Phukpattaranont, and E. S. Ebbini, "Detection and mapping of thermal lesions using dual-mode ultrasound phased array," in *Proc. IEEE Ultrason. Symp.*, 2002, pp. 1435–1438.

[24] J. U. A. Kluiwstra, T. Tokano, J. Davis, S. A. Strickberger, and C. A. Cain, "Real time image guided high intensity focused ultrasound for myocardial ablation: In vivo study," in *Proc. IEEE Ultrason. Symp.*, 1997, pp. 1327–1330.

[25] H. Wan, P. VanBaren, E. S. Ebbini, and C. A. Cain, "The ultrasound surgery: Comparison of strategies using phased array systems," *IEEE Trans. Ultrason., Ferroelect., Freq. Contr.*, vol. 43, pp. 1085–1098, 1996.

[26] I. H. Rivens, R. L. Clarke, and G. R. ter Haar, "Design of focused ultrasound surgery transducers," *IEEE Trans. Ultrason., Ferroelect., Freq. Contr.*, vol. 43, pp. 1023–1031, 1996.

[27] R. J. Dickinson and R. I. Kitney, "Miniature ultrasonic probe construction for minimal access surgery," *Phys. Med. Biol.*, vol. 49, pp. 3527–3528, 2004.

[28] J. E. Zimmer, K. Huynynen, F. Marcus, and D. S. He, "The feasibility of using ultrasound for cardiac ablation," *Proc. IEEE Ultrason. Symp.*, pp. 1203–1206, 1993.

[29] D. S. He, J. E. Zimmer, K. Hynynen, F. I. Marcus, A. C. Caruso, L. F. Lampe, and M. L. Aguirre, "Application of ultrasound energy for intracardiac ablation of arrhythmias," *Eur. Heart J.*, vol. 16, pp. 961–966, 1995.

[30] A. Natale, E. Pisano, J. Shewchik, D. Bash, R. Fanelli, D. Potenza, P. Santarelli, R. Schweikert, R. White, W. Saliba, L. Kanagaratnam, P. Tchou, and M. Lesh, "First human experience with pulmonary vein isolation using a through-the-balloon circumferential ultrasound ablation system for recurrent atrial fibrillation," *Circulation*, vol. 102, pp. 1879–1882, 2000.

[31] C. I. Zanelli, C. W. Hennige, and N. T. Sanghvi, "Design and characterization of a 10 cm annular array transducer for high intensity focused ultrasound (HIFU) applications," in *Proc. IEEE Ultrason. Symp.*, 1994, pp. 1887–1890.

[32] L. A. Frizzell, S. A. Goss, J. T. Kouzmanoff, and J. M. Yang, "Sparse random ultrasound array for focal surgery," in *Proc. IEEE Ultrason. Symp.*, 1996, pp. 1319–1323.

[33] F. Dupenloup, J. Y. Chapelon, D. J. Cathignol, and O. A. Sapozhnikov, "Reduction of the grating lobes of annular arrays used in focused ultrasound surgery," *IEEE Trans. Ultrason., Ferroelect., Freq. Contr.*, vol. 43, pp. 991–998, 1996.

[34] J. U. Kluiwstra, Y. Zhang, P. VanBaren, S. A. Strickberger, E. S. Ebbini, and E. S. Cain, "Ultrasound phased arrays for noninvasive myocardial ablation: Initial studies," in *Proc. IEEE Ultrason. Symp.*, 1995, pp. 1605–1608.

[35] M. D. Lesh, J. M. Kalman, and M. R. Karch, "Use of intracardiac echocardiography during electrophysiologic evaluation and therapy of atrial arrhythmias," *J. Cardiovasc. Electrophysiol.*, vol. 9, Suppl., pp. S40–S47, 1998.

[36] J. E. Olgin, J. M. Kalman, M. Chin, C. Stillson, M. Maguire, P. Ursel, and M. D. Lesh, "Electrophysiological effects of long, linear atrial lesions placed under intracardiac ultrasound guidance," *Circulation*, vol. 96, pp. 2715–2721, 1997.

[37] L. M. Epstein, M. A. Mitchell, T. W. Smith, and D. E. Haines, "Comparative study of fluoroscopy and intracardiac echocardiographic guidance for the creation of linear atrial lesions," *Circulation*, vol. 98, pp. 1796–1801, 1998.

[38] S. Vaezy, M. Andrew, P. Kackowski, and L. Crum, "Image-guided acoustic therapy," *Annu. Rev. Biomed. Eng.*, vol. 3, pp. 375–390, 2001.

[39] S. Vaezy, X. Slu, R. W. Martin, E. Chi, P. I. Nelson, M. R. Bailey, and L. A. Crum, "Real-time visualization of high-intensity focused ultrasound treatment using ultrasound imaging," *Ultrasound Med. Biol.*, vol. 27, pp. 33–42, 2001.

[40] D. N. Stephens, K. K. Shung, J. Cannata, J. Zhao, R. Chia, H. Nguyen, K. Thomenius, A. Dentinger, D. G. Wildes, X. Chen, M. O'Donnell, R. I. Lowe, J. Pemberton, G. H. Burch, and D. J. Sahn, "Clinical application and technical challenges for intracardiac ultrasound imaging," in *Proc. IEEE Ultrason. Symp.*, 2004, pp. 772–779.

[41] K. Thomenius, A. Dentinger, K. K. Shung, R. Chia, D. N. Stephens, M. O'Donnell, R. I. Lowe, C. H. Davies, G. H. Burch, and D. J. Sahn, "A new high frequency intracardiac imaging technology with improved resolution and steerability facilitates motion mapping and EP electrodes for rhythm analysis," presented at Amer. Heart Assoc. Annu. Sci. Sessions, Nov. 7–10, 2004, New Orleans, LA.

[42] K. L. Gentry and S. W. Smith, "Integrated catheter for 3-D intracardiac echocardiography and ultrasound ablation," *IEEE Trans. Ultrason., Ferroelect., Freq. Contr.*, vol. 51, pp. 800–808, 2004.

[43] A. Hammoude, "Edge detection in ultrasound images based on differential tissue attenuation rates," *Ultrason. Imag.*, vol. 21, pp. 31–42, 1999.

[44] J. Y. Chapelon, J. Margonari, D. Cathignol, S. Gelet, C. Guers, and Y. Theillere, "Threshold for tissue ablation by focused ultrasound," in *Proc. IEEE Ultrason. Symp.*, 1990, pp. 1653–1655.

[45] C. Damianou and K. Hynynen, "The effect of various physical parameters on the size of necrosed tissue volume during ultrasound surgery," *J. Acoust. Soc. Amer.*, vol. 95, pp. 1641–1649, 1994.

[46] G. ter Haar, "Ultrasound focal beam surgery," *Ultrasound Med. Biol.*, vol. 25, pp. 1089–1100, 1995.

[47] H. T. O'Neil, "Theory of focusing radiators," *J. Acoust. Soc. Amer.*, vol. 21, pp. 516–526, 1949.

[48] E. B. Hutchinson, M. T. Buchanan, and K. Hynynen, "Design and optimization of an aperiodic ultrasound phased array for intracavitary prostate thermal therapies," *Med. Phys.*, vol. 23, no. 5, pp. 767–776, 1996.

[49] W. N. McDicken, *Diagnostic Ultrasonics: Principles and Use of Instruments*. 3rd ed. New York: Churchill Livingstone, 1991.

[50] A. Macovski, *Medical Imaging Systems*. Englewood Cliffs, NJ: Prentice-Hall, 1983.

[51] N. C. Bhavaraju, H. Cao, D. Yuan, J. W. Valvano, and J. G. Webster, "Effective thermal properties of normal and ablated swine myocardium," in *Proc. IEEE Eng. Med. Biol.*, 1997, pp. 148–151.

[52] B. E. Billard, K. Hynynen, and R. B. Roemer, "Effects of physical parameters on high temperature ultrasound hyperthermia," *Ultrasound Med. Biol.*, vol. 16, pp. 409–420, 1990.

[53] C. Tangwongsan, J. A. Will, J. G. Webster, K. L. Meredith, and D. M. Mahvi, "In vivo measurement of swine endocardial convective heat transfer coefficient," *IEEE Trans. Biomed. Eng.*, vol. 51, pp. 1478–1486, 2004.

[54] I. D. Santos, J. A. Will, A. F. da Rocha, F. A. de O Nascimento, J. G. Webster, and J. W. Valvano, "In vivo measurements of heat transfer on the endocardial surface," *Physiol. Measure.*, vol. 24, pp. 321–335, 2003.

[55] S. A. Sapareto and W. C. Dewey, "Thermal dose determination in cancer therapy," *Int. J. Radiol. Oncol. Biol. Phys.*, vol. 10, pp. 787–800, 1984.

[56] D. Haemmerich, J.G. Webster, and D. M. Mahvi, "Thermal dose versus isotherm as lesion boundary estimator for cardiac hepatic radio-frequency ablation," in *Proc. IEEE Eng. Med. Biol.*, 2003, pp. 134–136.

[57] C. Diederich and K. Hynynen, "The feasibility of electrically focused ultrasound to induce deep hyperthermia in cavities," *IEEE Trans. Ultrason., Ferroelect., Freq. Contr.*, vol. 38, pp. 207–219, 1991.

[58] S. Ho, D. Sanchez-Quintana, J. A. Cabrera, and R. H. Anderson, "Anatomy of the left atrium: Implications for radiofrequency ablation of atrial fibrillation," *J. Cardiovasc. Electrophysiol.*, vol. 10, pp. 1525–1533, 1999.

[59] M. McDonald, S. Lochhead, R. Chopra, and M. J. Bronskill, "Multimodality tissue-mimicking phantom for thermal therapy," *Phys. Med. Biol.*, vol. 49, pp. 2767–2778, 2004.

[60] E. S. Ebbini, C. Simon, H. Lee, and W. Choi, "Self-guided ultrasound phased arrays for noninvasive surgery," in *Proc. SPIE*, vol. 4247, 2001, pp. 30–40.

[61] A. L. Malcolm and G. ter Haar, "Ablation of tissue volumes using high intensity focused ultrasound," *Ultrasound Med. Biol.*, vol. 22, pp. 659–669, 1996.

[62] G. Kino, *Acoustic Waves: Devices, Imaging, and Analog Signal Processing*. Englewood Cliffs, NJ: Prentice-Hall, 1987.

[63] C. Simon, P. VanBaren, and E. Ebbini, "Combined imaging and therapy with piezocomposite phased array," in *Proc. IEEE Ultrason. Symp.*, 1998, pp. 1555–1558.

Serena H. Wong is from Menlo Park, CA. She received her B.S. and M.S. degrees in electrical engineering from Stanford University (Stanford, CA) and is currently pursuing her Ph.D. degree there.

She has been part of the Medical Imaging Group since her sophomore year in college, and has been working on high-intensity, focused ultrasound for the past 3 years.

She is a National Science Foundation Fellow (2002), Stanford Graduate Fellow, and a member of Tau Beta Pi (2001).

Greig C. Scott is from Canada. He did his undergraduate work in electrical engineering in the co-op program in the University of Waterloo (Waterloo, Ontario, Canada). He completed his M.S. and Ph.D. degrees at the University of Toronto (Toronto, Ontario, Canada).

He has been a senior research associate in the Medical Imaging Group for 8 years, and he has been instrumental in the development, design, and construction of the Prepolarized MRI System.

Steven M. Conolly is from Rochester, NY. He completed his M.S. and Ph.D. degrees at Stanford University, Stanford, CA, in MRI RF pulse design.

He has been a senior research associate in the Medical Imaging Group for 8 years, and he has been instrumental in the development, design, and construction of the Prepolarized MRI System. He is now a Professor of Bioengineering at the University of California, Berkeley.

Girish Narayan did his undergraduate work at MIT, Cambridge, MA, in computer science, but then he went to medical school. He is currently a Fellow in Cardiovascular Medicine at Stanford University, Stanford, CA.

David H. Liang is from Hawaii. He completed his B.S. degree in electrical engineering at MIT, Cambridge, MA. He completed the Stanford University, Stanford, CA, M.D./Ph.D. program with a Ph.D. degree in electrical engineering on cochlear implants.

He is currently an assistant professor of cardiovascular medicine and courtesy in electrical engineering. His primary research focuses on look-ahead ultrasound and intracardiac devices.